STUDY ON FLOW AND HEAT TRANSFER PERFORMANCE OF SINGLE JET IMPINGEMENT COOLING THROUGH VARIABLE-DIAMETER HOLE

Lei Xi, Qicheng Ruan, Yuan Gao, Jianmin Gao, Liang Xu*, Yunlong Li

School of Mechanical Engineering, Xi'an Jiaotong University, Xi'an 710049, Shaanxi, China

* Corresponding author; E-mail: xilei100@mail.xjtu.edu.cn

In this work, the heat transfer and flow characteristics of single jet impinging cooling with three types of hole configurations, namely converging hole, straight hole, and expanded hole, were compared and analyzed numerically. The influence laws of Reynolds number, outlet-to-inlet diameter ratio, and impinging height ratio on the heat transfer, flow, and comprehensive thermal performance of the converging-hole impinging cooling were intensively investigated. Finally, the empirical correlations were fitted and the sensitivity of performance variables to influencing parameters were analyzed for the converging-hole impinging cooling. The results show that the converging hole exhibits the superlative heat transfer performance but the poorest flow performance. The expanded hole exhibits the poorest heat transfer performance but the superlative flow performance. As Re > 24,000, the comprehensive thermal performance of the three types of hole configurations is similar. For the converging-hole impinging cooling, when Re increases from 6,000 to 30,000 under various structural parameters, the average Nusselt number increases by approximately 1.62 to 2.65 times, and the comprehensive thermal coefficient increases by approximately 1.58 to 2.45 times. As the outlet-to-inlet diameter ratio increases from 0.5 to 0.9 under various Re, the pressure loss coefficient of the converging-hole impinging cooling decreases by approximately 91.47% to 92.95%, and the corresponding average Nusselt number decreases by 43.61% to 60.07%. When the impinging height ratio is 2.0, the converging-hole impinging cooling exhibits lower pressure loss coefficients. The parameter sensitivity analysis shows that the average Nusselt number of converging-hole impinging cooling is sensitive to changes in the outlet-to-inlet diameter ratio and Reynolds number, but insensitive to changes in the impinging height ratio. The pressure loss coefficient is highly sensitive to changes in the outlet-to-inlet diameter ratio, but insensitive to changes in the Reynolds number and impinging height ratio. The comprehensive thermal coefficient is highly sensitive to changes in the Reynolds number, but insensitive to changes in the outlet-to-inlet diameter ratio and impinging height ratio.

Key words: *impinging cooling, single jet, variable-diameter hole, flow performance, heat transfer performance*

1. Introduction

The modern gas turbine rotor inlet temperature has already exceeded 1,700°C [1], far exceeding the upper limit of heat resistance of blade material [2]. This poses a great challenge to the safe and reliable operation of gas turbines, hence there is an urgent need to study efficient turbine blade cooling

technologies. Impinging cooling is one of the most efficient approaches to enhance the local cooling effectiveness of turbine blade inner walls. To achieve impinging cooling, essential impinging baffles with an array of small holes are generally arranged inside the turbine blades [3]. Therefore, impinging cooling is typically applied in areas of turbine blades with high thermal loads and ample space, such as the turbine blade mid-chord region or leading-edge region [4].

In turbine blades, traditional jet impinging holes are mostly equal-diameter circular holes [5]. Currently, a large number of literature reports have focused on numerical and experimental investigations regarding the cooling characteristics and capability of jet impinging cooling with equal-diameter circular holes [6]. These studies mainly analyze the effects of arrangement methods, operating conditions, and structural parameters on the cooling characteristics and capability of impinging cooling, and conduct optimization designs [7]. The arrangement methods mainly include perpendicular jet holes to the target wall [8], inclined jet holes to the target wall [9], single hole arrangement [10], array holes arrangement [11], and other forms. The operating conditions and structural parameters mainly include Reynolds number, inlet temperature, wall heat flux [12], impinging height, hole diameter, hole spacing, hole inclination angle, etc. [13]. Additionally, some researchers have inserted spiral strips into circular jet holes [14] or processed the inner wall surface of circular jet holes into a helical shape [15], thereby forming swirling jets to further improve the cooling capability of jet impinging.

The aforementioned research indicates that raising Reynolds number or changing jet hole structure to increase the jet impinging velocity on the target wall is one of the important factors for enhancing the heat transfer effectiveness of impinging cooling [16-17]. Changing the jet hole outlet diameter also affects the velocity and distribution of jet impinging on the target wall, thus influencing the heat transfer and flow performance of impinging cooling [18]. Therefore, in recent years, some investigators have started to focus on the effect of hole diameter variation (variation in inlet and outlet cross-section of the hole) on the heat transfer and flow characteristics and capability of impinging cooling [19], and have conducted some preliminary studies. Shuja et al. [20] analyzed the heat transfer and flow distribution behaviors of converging jet impinging on conical holes through numerical methods. The study indicated that the pressure loss coefficient and heat transfer coefficient both reach their highest values at the wall in the inlet and outlet areas of the conical hole. Carcasci et al. [21] compared the heat transfer capability of circular straight holes, circular inclined holes, and converging inclined holes through experimental methods. Their findings indicated that the heat transfer level of impinging cooling using converging inclined holes increases by about 10% to 20%, as compared with circular straight holes. Ram and Sivamani [22-23] analyzed the heat transfer characteristics of converging-hole impinging cooling by numerical calculation at different Reynolds numbers. They pointed out that converging-hole impinging cooling has higher heat transfer capability than that of straight-hole impinging cooling. Sathish et al. [24] researched the effect of angle (10°, 20°, and 30°) of converging holes on the performance of impinging cooling at turbine blade leading-edge through numerical simulation. Their results showed that compared to the straight-hole impinging cooling, the converging-hole impinging cooling has better heat transfer performance. Zielinski et al. [25-26] carried out experimental investigation on the flow characteristics of impinging cooling using variable-diameter holes. The study indicated that compared to jet impinging cooling using equal-diameter hole, the jet impinging cooling using variable-diameter hole can effectively enhance the fluid flow momentum and achieve a heat transfer enhancement of about 35%. Chi et al. [27] conducted structural optimization design of variable-diameter jet hole under non-uniform thermal load conditions on the target wall. They obtained multiple sets of optimal structural parameter combinations that result in more even distribution of temperature on target wall.

Although some researchers have studied the heat transfer and flow behaviors of jet impinging using variable-diameter holes, most of these studies only focus on the effects of variable-diameter holes on the heat transfer enhancement of jet impinging cooling. Few researchers have investigated the influence of variable-diameter holes on the flow performance and comprehensive thermal performance of impinging cooling. Generally, the enhancement of heat transfer is inevitably accompanied by increased pressure loss and weakened flow performance. Therefore, in addition to heat transfer performance, it is essential to assess the overall capability of impinging cooling using

variable-diameter hole based on flow performance and comprehensive thermal performance.

To address the aforementioned issue, this study investigated the heat transfer and flow capabilities of impinging cooling using variable-diameter holes. Firstly, numerical calculation approach was used to compare and analyze the heat transfer and flow behaviors and performance of three different hole configurations (i.e., converging hole with D_2/D_{in} = 0.5, straight hole with D_2/D_{in} = 1, and expanded hole with D_2/D_{in} = 1.5) under different Reynolds numbers. Then, the effects of Reynolds number (*Re*, ranging from 6,000 to 30,000), outlet-to-inlet diameter ratio (D_2/D_{in}, ranging from 0.5 to 0.9), and impinging height ratio (H/D_{in}, ranging from 1 to 4) on the heat transfer, flow, and comprehensive thermal performance of converging-hole impinging cooling were explored. Empirical correlations for the average Nusselt number, pressure loss coefficient, and comprehensive thermal coefficient of converging-hole impinging cooling were derived based on the Reynolds number, outlet-to-inlet diameter ratio, and impinging height ratio. Furthermore, the sensitivity of the performance variables of converging-hole impinging cooling to its input variables was analyzed. The research object and content of this article mainly focus on industrial applications of power equipment such as gas turbines and aviation engines. The research findings can provide valuable insights for the design of impinging cooling using variable-diameter holes in future advanced gas turbine blades.

2. Research object

The geometric model of the studied single jet impinging cooling using variable-diameter holes is displayed in Fig. 1. The model includes the straight-hole section and variable-diameter section of the jet hole, the impinging zone, and the solid target wall. The solid target wall has a square cross-section with a width of W = 100 mm and a thickness of δ = 3 mm. The total jet hole length is 20 mm, for which the first half being the straight-hole section of length H_1 = 10 mm and a diameter of D_{in} = 10 mm. The D_{in} is chosen as the characteristic length for calculating pressure loss coefficient, Nusselt number, Reynolds number, etc. The second half of the jet hole is the variable-diameter section of length H_2 = 10 mm. The jet hole diameter at the transition point is $D_1 = D_{in}$ = 10 mm. The hole outlet diameter D_2 is the variable under investigation, ranging from 5 mm to 15 mm. The corresponding jet hole outlet-to-inlet diameter ratio (D_2/D_{in}, ratio of hole outlet diameter to hole inlet diameter) ranges from 0.5 to 1.5. Where $0.5 \leq D_2/D_{in} < 1$ represents converging hole, D_2/D_{in} = 1 represents straight hole, and D_2/D_{in} = 1.5 represents expanded hole. Under a fixed impinging height H = 10 mm, the heat transfer and flow behaviors of impinging cooling were compared for the converging hole (D_2/D_{in} = 0.5), straight hole (D_2/D_{in} = 1.0), and expanded hole (D_2/D_{in} = 1.5). Because of the superior heat transfer capability of converging hole, this work particularly focuses on investigating the effects of different outlet-to-inlet diameter ratios and impinging height ratios on the heat transfer and flow performance of converging-hole impinging cooling. The values of outlet-to-inlet diameter ratios D_2/D_{in} are set to 0.5, 0.6, 0.7, 0.8, and 0.9, corresponding to outlet diameters D_2 of 5mm, 6mm, 7mm, 8mm, and 9mm, respectively. The impinging height ratios (H/D_{in}, ratio of impinging height to jet hole inlet diameter) are set to 1, 2, 3, and 4, with impinging heights H of 10mm, 20mm, 30mm, and 40mm, respectively. It is worth noting that the geometry parameters are varied while keeping the inlet cross-section of the jet hole constant to ensure the same inlet Reynolds number for the jet with the same cooling air mass flow rate.

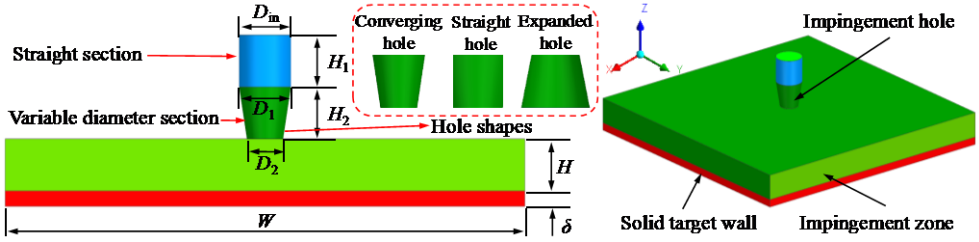

Fig. 1 Geometric Model

3. Research methods

3.1. Numerical calculation method

The heat transfer and flow behaviors of impinging cooling using variable-diameter holes were numerically solved using a steady-state, three-dimensional, and fluid-solid coupled approach in ANSYS CFX. The fluid-solid coupled computational model used in the study is shown in Fig. 2(a). It consists of several parts, including the fluid domains of the straight-hole section, variable-diameter section, and impinging region, as well as the solid domain of the impinging target surface. The interface between the solid domain and fluid domain was processed as a coupled interface, with the same temperature and heat flux on both sides. In the numerical calculations, merely the equation of heat conduction was computed in the solid domain. The fluid domain was presumed as incompressible and gravity-independent turbulent flow. The finite volume approach on the basis of finite element was used to discretize and solve the conservation equations of mass, momentum and energy. The RANS equations were employed to calculate the turbulent momentum equations, and the Total Energy equation was used to solve the heat transfer problem. High-precision discretization schemes were applied for the convective, source, and diffusion terms. The numerical solution was considered converged and stopped as the maximum residual value among all solved equations was below 10^{-6}.

The boundary conditions and parameters for the numerical calculations are as below: The inlet cooling air total temperature in the jet hole was set to 298.15 K. The inlet Reynolds number ranges from 6,000 to 30,000, corresponding to a cooling air velocity of 9.46 m/s to 47.31 m/s. The inlet cooling air turbulence intensity was designated to 5%. The outlet boundary of the computational domain was specified with a given static pressure, the mean value and floating range of which are 101 kPa and ± 5%. An even heat flux of 1,000 W/m^2 was given to the solid domain lower surface of the impinging target wall, which was the heated surface. The remaining surfaces were treated as no-slip and adiabatic walls. These boundary conditions were applied to simulate the heat transfer and flow behaviors of impinging cooling using variable-diameter holes.

The grid model for the numerical calculations is shown in Fig. 2(b). ANSYS ICEM was used to establish the grid model for the jet impinging cooling using variable-diameter holes. All computational domains were divided using the structured hexahedral mesh. The same division strategy was adopted for both the fluid and solid domains to minimize the numerical transmission errors between the meshes. The minimum mesh size was set as 0.05 mm. The total grid number was adjusted according to the maximum mesh size. The meshes near the wall surface were refined, with a mesh growth ratio of 1.2 and a first-layer mesh height of 0.001 mm. The above grid division method ensures that the wall y+ is close to 1. Additionally, local mesh refinement was performed for the jet hole and its surrounding impinging region to further enhance the accuracy of the numerical simulations.

Grid independence verification was conducted to assure the reliability and economy of the numerical approach for impinging cooling using variable-diameter holes. Five sets of grid models were examined in this work, with total mesh numbers of 500,000, 710,000, 1,010,000, 1,510,000, and 2,270,000. The specific case parameters for grid independence validation were set as Re = 18,000, D_2/D_{in} = 0.5, and H/D_{in} = 1. The results in Table 1 show that the mean Nusselt number on impinging target wall raises with the increment of mesh number. When the mesh number is about 1,510,000, further increasing the mesh number brings a negligible influence on the average Nusselt number, with a relative variation within 1.5%. This indicates that grid independence is achieved. Therefore, the grid models for the jet impinging cooling using variable-diameter holes of different configurations will adopt the same division strategy as the fourth set of grids (1,510,000 meshes).

Table 1 Grid independence validation.

No.	Total mesh number/million	Nu_{ave}	Relative difference/%
1	50	111.6	-
2	71	140.4	25.81
3	101	166.9	18.87
4	151	171.9	3.00
5	227	174.3	1.40

Numerical approach validation was also conducted to assure the accuracy of the numerical approach for impinging cooling using variable-diameter holes. Taking the test results of local Nusselt number for straight-hole impinging cooling in Reference [28] as an example, the exactitude of numerical approach in the present work was validated. The parameters Re = 12,000 and H/D_{in} = 2 were selected. Fig. 2(c) presents the comparison among local Nusselt numbers gained by numerical calculations in this study using k-ω, RNG k-ε, and SST k-ω models, and the corresponding test data in Reference [28]. From Fig. 2(c), it can be observed that the distribution tendency of local Nusselt numbers calculated by RNG k-ε model greatly differs from the test data, and within the range of $0 < R/D_{in} < 3$, its calculated values are much higher than the test data. The distribution trend of local Nusselt numbers calculated by k-ω turbulence model is also inconsistent with the test data to some extent, but the corresponding values are relatively close. The highest prediction deviation of k-ω model is approximately 16.37% when comparing the average values of local Nusselt numbers. The distribution trend and corresponding values of local Nusselt numbers computed by SST k-ω model are consistent to the test data. When comparing the mean values of local Nusselt numbers, the highest prediction deviation of SST k-ω model is approximately 5.89%. The above comparison indicates that the numerical approach in the current work, combined with SST k-ω model, can accurately simulate the heat transfer characteristics of single-hole jet impinging cooling. Thereby, the SST k-ω model was used for the numerical calculations of single-hole jet impinging cooling in all subsequent parts of this study.

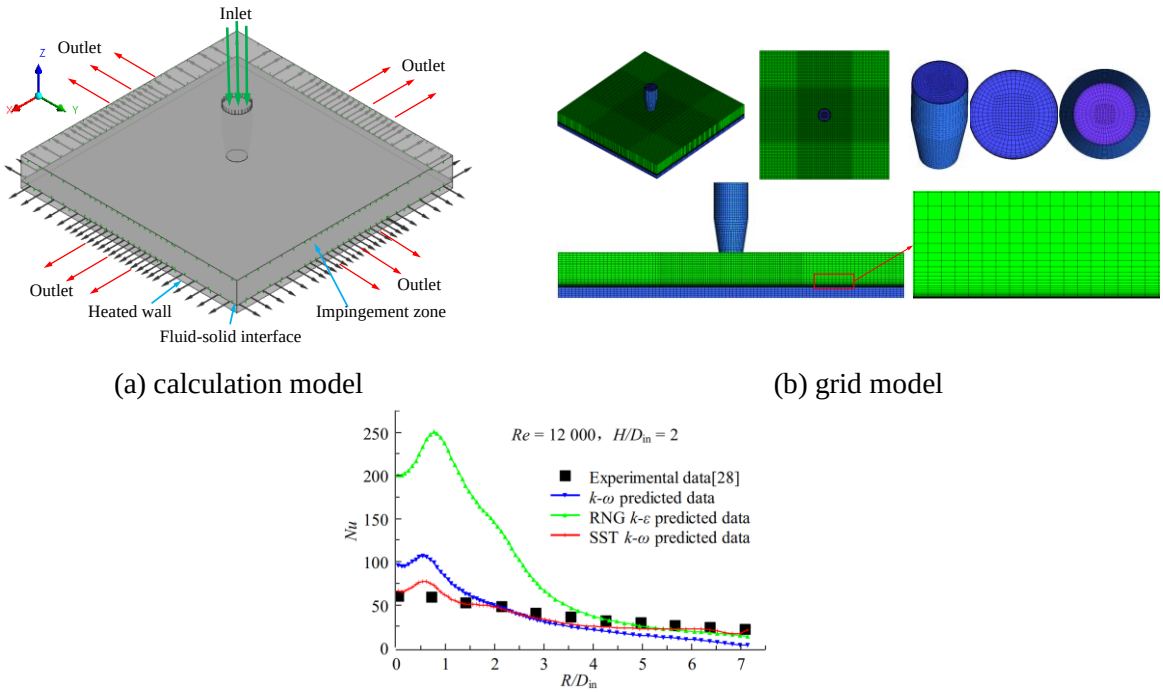

(a) calculation model (b) grid model

(c) Comparison of calculation results with experimental results

Fig. 2 Numerical simulation model and experimental validation

3.2. Parameter definition

The inlet Reynolds number (*Re*) for a jet hole is defined as:

$$Re = uD_{in} / v \tag{1}$$

where u represents the cooling air velocity at the inlet of jet hole in m/s, v is dynamic viscosity in Pa·s.

The local Nusselt number (*Nu*) based on the equivalent diameter of jet hole inlet is defined as:

$$Nu = qD_{in}/[(T_w - T_{in})\lambda] \tag{2}$$

where q represents the target wall heat flux in W/m^2, T_w represents the target wall temperature in K, T_{in} represents the cooling air temperature at jet hole inlet in K.

The pressure loss coefficient (C_p) is defined as:

$$C_p = 2(p_{in} - p_{out})/\rho u^2 \tag{3}$$

where p_{in} represents the area-averaged pressure at jet hole inlet in Pa, p_{out} represents the area-averaged pressure at the computational domain outlet in Pa.

The comprehensive thermal coefficient (G) is defined as [3, 31]:

$$G = Nu_{ave}/C_p^{1/3} \tag{4}$$

4. Result analysis and discussion

4.1. Comparison of impinging cooling performance of three types of holes

Fig. 3 shows the distributions of heat transfer and flow characteristics for impinging cooling using three different types of holes, when *Re* is 18,000 and H/D_{in} is 1. Fig. 3(a) displays the distributions of flow velocity and Fig. 3(b) displays the distributions of local *Nu*. As depicted in Fig. 3(a), the flow distribution characteristics of impinging cooling of the three types of holes are similar. Specifically, the cooling air flow velocity in the free jet zone is high. The cooling air flow velocity near target wall in the stagnation zone is very low. After that, the cooling air flow velocity near target wall in the wall jet zone first rapidly increases and then gradually decreases. Finally, a vortex with large size and low velocity is formed above the target surface near the target outlet side. As exhibited in Fig. 3(a), the cooling air velocities of converging-hole impinging cooling in the free jet zone and wall jet zone are significantly higher than those of straight-hole impinging cooling and expanded-hole impinging cooling in the corresponding zones. Especially in the zone near target wall in the wall jet zone with $R/D_{in} < 3$, the cooling air velocity of converging-hole impinging cooling is even higher. This phenomenon may bring higher C_p for the converging-hole impinging cooling. As exhibited in Fig. 3(b), the distribution characteristics of *Nu* on the target wall for impinging cooling using three different types of holes are relatively consistent. Because the direct impinging of high-speed jet destroys the heat transfer boundary layer around the stagnation point and increases the disturbance effect of the surrounding fluid, the *Nu* on the target wall directly below the impinging hole is very high, and a circular high heat transfer area is formed at the central region of target wall. After that, the *Nu* of target wall progressively drops along the radial direction of impinging hole, and four low heat transfer regions are formed in the four corners of target wall. As also exhibited in From Fig. 3(b), the *Nu* of target wall for converging-hole impinging cooling are significantly higher than those for straight-hole impinging cooling and expanded-hole impinging cooling. Especially in the high heat transfer region in the center region of target wall, the *Nu* of converging-hole impinging cooling improves more significantly. This is because the smaller outlet section of the converging hole makes the cooling air in the free jet zone impinge to the target wall at a higher flow velocity, and also effectively improves the cooling air velocity near target wall in the wall jet zone, thereby improving the local heat transfer

performance of the target wall. In addition, the *Nu* of target wall of straight-hole impinging cooling is also higher than that of expanded-hole impinging cooling. This is because the larger outlet section of expanded hole reduces the cooling air flow velocity in the free jet zone and wall jet zone, weakening the disturbance of the cooling air and the damage to the boundary layer, thus reducing the local heat transfer performance of target wall.

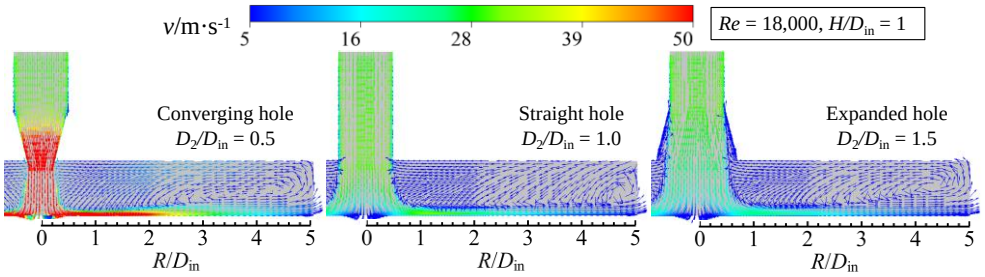

(a) flow velocity distribution

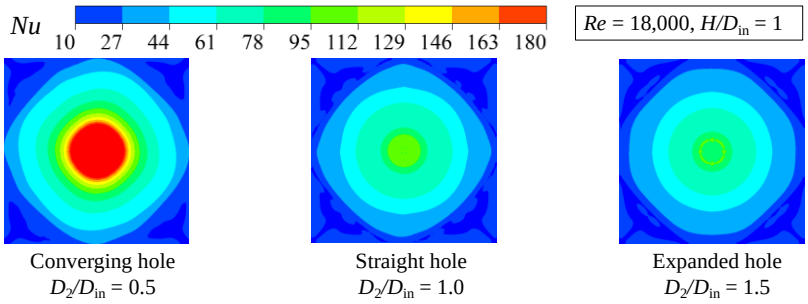

(b) local *Nu* distribution

Fig. 3 Heat transfer and flow characteristics distribution for three different hole configurations

In general, the heat transfer capability of converging-hole impinging cooling is the best, followed by straight-hole impinging cooling, while the heat transfer capability of expanded-hole impinging cooling is the worst.

Fig. 4 shows the comparison of heat transfer and flow performance for impinging cooling using three different types of holes. Fig. 4(a) shows the C_p distribution, Fig. 4(b) shows the *Nu* distribution on target wall, Fig. 4(c) shows the Nu_{ave} distribution on target wall, and Fig. 4(d) shows the *G* distribution, where Nu_{ave} is the area-averaged *Nu*. As drawn in Fig. 4(a), under various *Re*, the C_p of straight-hole impinging cooling and expanded-hole impinging cooling is close, but the C_p of straight-hole impinging cooling is relatively higher. The C_p of converging-hole impinging cooling is significantly higher than that of straight-hole impinging cooling and expanded-hole impinging cooling, and this phenomenon is more obvious with the increment of *Re*. Specifically, when *Re* raises from 6,000 to 30,000, the C_p of converging-hole impinging cooling is about 16.67 to 21.09 times higher than that of straight-hole impinging cooling. The C_p of expanded-hole impinging cooling are 22.55% to 33.68% lower than that of straight-hole impinging cooling. Therefore, the flow performance of expanded-hole impinging cooling is the best, followed by straight-hole impinging cooling, and the flow performance of converging-hole impinging cooling is the worst. As exhibited in Fig. 4(b), the *Nu* of straight-hole impinging cooling and expanded-hole impinging cooling is close in whole target wall. While comparatively, the *Nu* of straight-hole impinging cooling is higher than that of expanded-hole impinging cooling. Compared with the *Nu* of straight-hole impinging cooling and expanded-hole impinging cooling, the *Nu* of converging-hole impinging cooling has very high increase amplitudes in the range of $-3 < R/D_{in} < 3$, with the maximum increase rate of 3.26 times (relative to straight hole) and 3.82 times (relative to expanded hole), respectively. The increase amplitudes of *Nu* of converging-hole impinging cooling in the ranges of $R/D_{in} < -3$ and $R/D_{in} > 3$ are small, about 28.08%

(relative to straight hole) and 39.01% (relative to expanded hole), respectively. From Fig. 4(c), it can be found that under various *Re*, the Nu_{ave} of target wall of converging-hole impinging cooling is significantly higher than that of straight-hole impinging cooling and expanded-hole impinging cooling. The Nu_{ave} of target wall of straight-hole impinging cooling and expanded-hole impinging cooling is close. While comparatively, the Nu_{ave} of target wall of straight-hole impinging cooling is also slightly higher than that of expanded-hole impinging cooling. Specifically, when *Re* is 6,000 to 30,000, the Nu_{ave} of target wall of converging-hole impinging cooling is about 0.96 to 1.85 times higher than that of straight-hole impinging cooling. The Nu_{ave} of target wall of expanded-hole impinging cooling is reduced by about 5.62% to 10.85% compared with that of straight-hole impinging cooling. Therefore, the heat transfer capability of converging-hole impinging cooling is the best, followed by straight-hole impinging cooling, while the heat transfer capability of expanded-hole impinging cooling is the worst. From Fig. 4(d), it can be observed that when *Re* is less than 24,000, the expanded-hole impinging cooling exhibits the highest *G*, followed by straight-hole impinging cooling, while the converging-hole impinging cooling shows the lowest *G*. This indicates that when *Re* is less than 24,000, the expanded-hole impinging cooling has the best comprehensive thermal performance, next is straight-hole impinging cooling, while the converging-hole impinging cooling has the poorest comprehensive thermal performance. However, when *Re* is equal to or greater than 24,000, the *G* of impinging cooling under the three types of hole configurations is very similar, indicating a close similarity in their comprehensive thermal performance.

Because the converging-hole impinging cooling can bring great heat transfer enhancement, the subsequent content of this investigation will research the heat transfer and flow performance of converging-hole impinging cooling at different parameters.

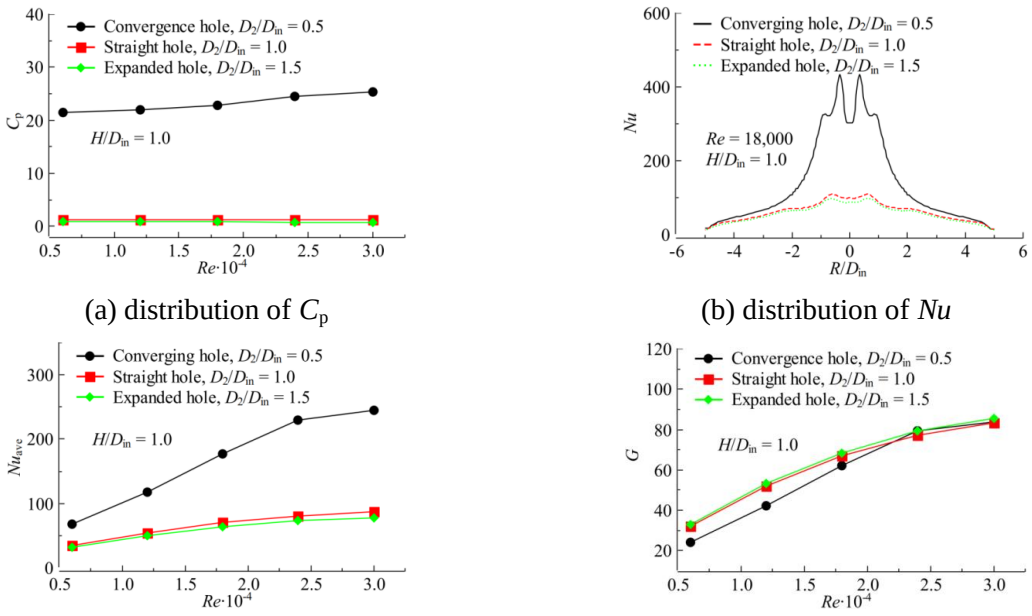

(a) distribution of C_p

(b) distribution of Nu

(c) distribution of Nu_{ave}

(d) distribution of G

Fig. 4 Comparison of heat transfer and flow performance for three different hole configurations

4.2. Flow performance analysis of converging-hole impinging cooling

Fig. 5 depicts the flow distributions of converging-hole impinging cooling under different parameters. As depicted in Fig. 5(a), when *Re* = 6,000, two vortexes with opposite directions appear in the wall jet zone of converging-hole impinging cooling. Taking the zone on the right side of the impinging hole as an example, the rotation direction of the vortex near the impinging hole is counterclockwise and the size is large, and the rotation direction of vortex near the outlet side is clockwise and the size is small. As *Re* raises from 12,000 to 30,000, only one large-scale

counterclockwise vortex appears in the wall jet zone of converging-hole impinging cooling, and the size of the vortex almost remains unchanged under various *Re*. As also depicted in Fig. 5(a), with the increment of *Re*, the range of high velocity region in the wall jet zone gradually increases. As can be found from Fig. 5(b), when D_2/D_{in} is 0.5 to 0.8, the position and size of vortex in the wall jet zone of converging-hole impinging cooling do not significantly change. When D_2/D_{in} is 0.9, the size of vortex in the wall jet zone significantly decreases, and the position is closer to the target wall and target outlet. Besides, with the increase of D_2/D_{in}, the cooling air velocity near target wall in the free jet zone and wall jet zone significantly decreases, and the range of high velocity region in the wall jet zone also gradually decreases. As can be found from Fig. 5(c), with the increment of H/D_{in}, the size of vortex in the wall jet zone of converging-hole impinging cooling becomes larger and larger, while the width of high velocity cooling air region in the free jet zone gradually decreases. Specifically, as H/D_{in} increases from 0.5 to 4, the corresponding width of high velocity cooling air region in the free jet zone decreases from the range of $R/D_{in} \approx 0.39$ to the range of $R/D_{in} \approx 0.34$. Besides, with the increment of H/D_{in}, the range of high velocity region in the wall jet zone also gradually decreases.

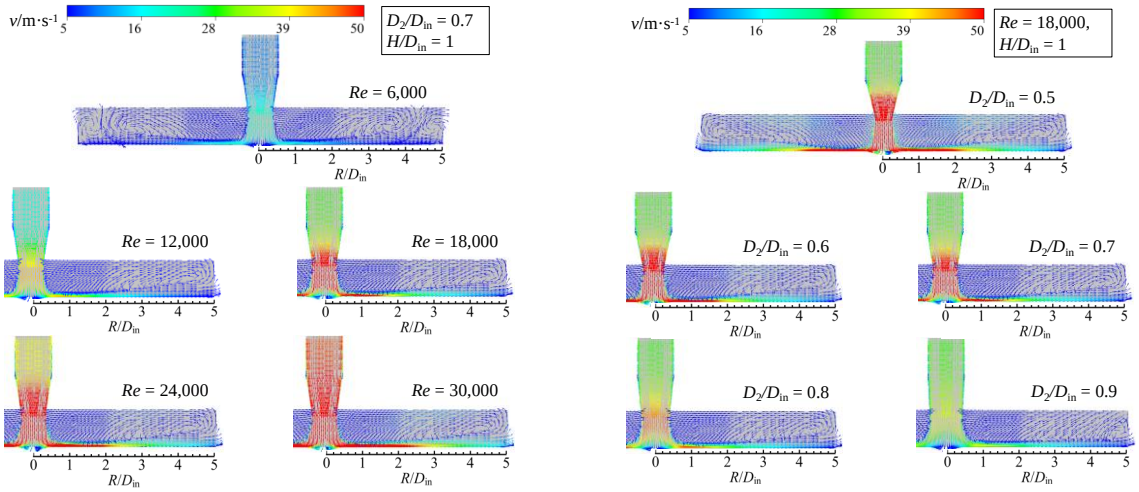

(a) effect of *Re*

(b) effect of D_2/D_{in}

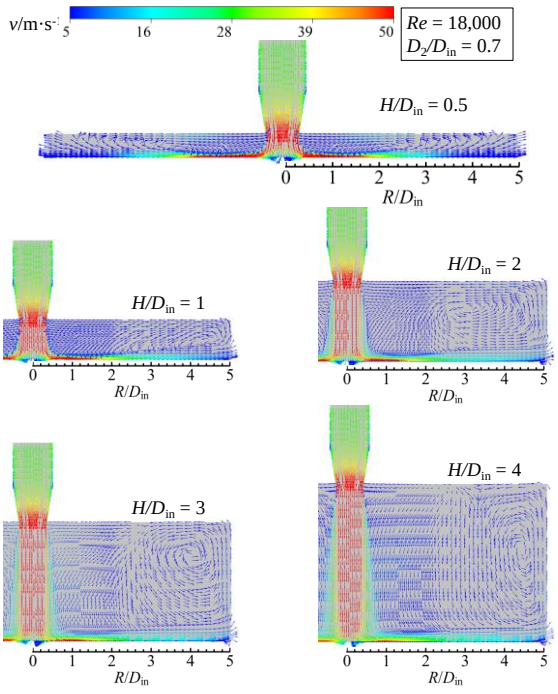

(c) effect of H/D_{in}

Fig. 5 Flow distribution of converging-hole impinging cooling under different parameters

Fig. 6 depicts the variation curves of C_p of converging-hole impinging cooling under different parameters. As depicted in Fig. 6(a), for cases D_2/D_{in} = 0.5 and H/D_{in} = 1, the increment of *Re* increases the C_p of converging-hole impinging cooling to a certain extent (as *Re* raises from 6,000 to 30,000, the C_p increases by 18.26%), and reduce its flow performance. Except for case at D_2/D_{in} = 0.5 and H/D_{in} = 1, the increase of *Re* indistinctively affects the C_p (i.e. flow performance) of converging-hole impinging cooling. As displayed in Fig. 6(b), under various *Re*, with the increase in D_2/D_{in}, the C_p of converging-hole impinging cooling rapidly decreases. This is because when the inlet section of impinging hole is fixed, the outlet section of impinging hole is smaller when the D_2/D_{in} is small. This makes the cooling air velocity near target wall in the free jet zone and the wall jet zone very high, thus increasing the C_p in the whole process of jet impinging. When the D_2/D_{in} raises, the outlet section of impinging hole synchronously raises, and the cooling air velocity near target wall in the corresponding free jet zone and wall jet zone significantly decreases, thus reducing the C_p in the whole jet impinging process. Specifically, compared with D_2/D_{in} = 0.5, the C_p of converging-hole impinging cooling at D_2/D_{in} = 0.9 is reduced by about 91.47% to 92.95% at various *Re*. Therefore, the increase of D_2/D_{in} can effectively improve the flow performance of converging-hole impinging cooling. As illustrated in Fig. 6(c), when H/D_{in} is less than 2.0, the increase of H/D_{in} under different *Re* significantly reduces the C_p of converging-hole impinging cooling. When H/D_{in} is greater than 2.0, increasing H/D_{in} indistinctively affects the C_p of converging-hole impinging cooling, and the variation laws of C_p are not completely consistent under different *Re*. On the whole, when H/D_{in} is 2.0, the C_p of converging-hole impinging cooling is lower and the flow performance is better.

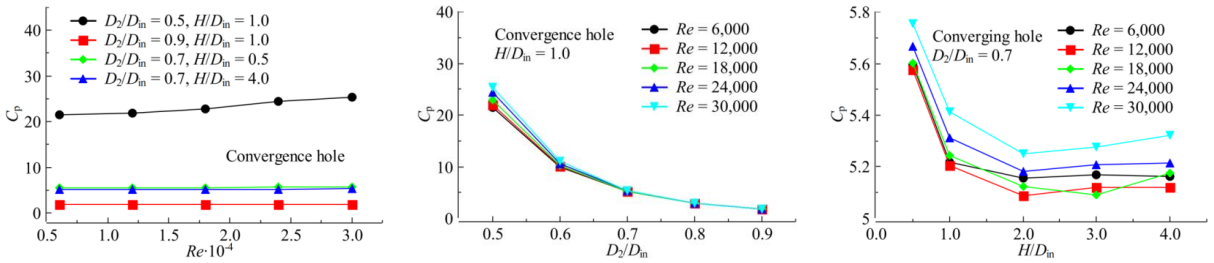

(a) effect of *Re* (b) effect of D_2/D_{in} (c) effect of H/D_{in}

Fig. 6 Variation curves of C_p of converging-hole impinging cooling under different parameters

4.3. Heat transfer performance analysis of converging-hole impinging cooling

Fig. 7 displays the distributions of *Nu* of converging-hole impinging cooling under different parameters. As illustrated in Fig. 7, the distribution characteristics of *Nu* on target wall of converging-hole impinging cooling under different parameters are similar. Specifically, a circular high *Nu* region is formed at the central region of target wall, and four low *Nu* regions are formed at the four corners of target wall. As for the influence of *Re*, it is shown in Fig. 7(a) that with the increment of *Re*, the range of high *Nu* region on target wall of converging-hole impinging cooling significantly increases. This shows that the increment of *Re* can greatly improve the heat transfer performance of whole target wall, especially in the central region of target wall. It is because the increment of *Re* strengthens the cooling air velocity near the target wall in the free jet zone and the wall jet zone (as depicted in Fig. 5(a)), intensifies the heat exchange between the target wall and the cooling air, and thereby improves the heat transfer effect of target wall. As for the influence of D_2/D_{in}, it is shown in Fig. 7(b) that with the increment of D_2/D_{in}, the range of high *Nu* region on target wall of converging-hole impinging cooling significantly decreases. This shows that increasing D_2/D_{in} will weaken the heat transfer performance of whole target wall, particularly the heat transfer performance of target wall central region. This is because the increase of D_2/D_{in} reduces the cooling air velocity near the target wall in the free jet zone and the wall jet zone ($-2.5 < R/D_{in} < 2.5$) (as shown in Fig. 5(b)), thereby weakening the local heat transfer capacity of target wall. As for the H/D_{in}, it is

illustrated in Fig. 7(c) that with the increment of H/D_{in}, the range of the highest *Nu* region (red circle) on target wall of converging-hole impinging cooling slightly increases, while the range of the second highest *Nu* region (yellow circle) gradually decreases. This is mainly because the distribution state of the cooling air velocity in the free jet zone (as shown in Fig. 5(c)) changes with the change of H/D_{in}. It is worth noting that when H/D_{in} = 2, a red ring in the high *Nu* area appears outside the red circle in the center of the target wall. That is, when H/D_{in} = 2, the *Nu* of the target wall shows a trend of first decreasing, then increasing, and then decreasing outward from the center. On the whole, the H/D_{in} inconspicuously impacts the local heat transfer performance of target wall of converging-hole impinging cooling.

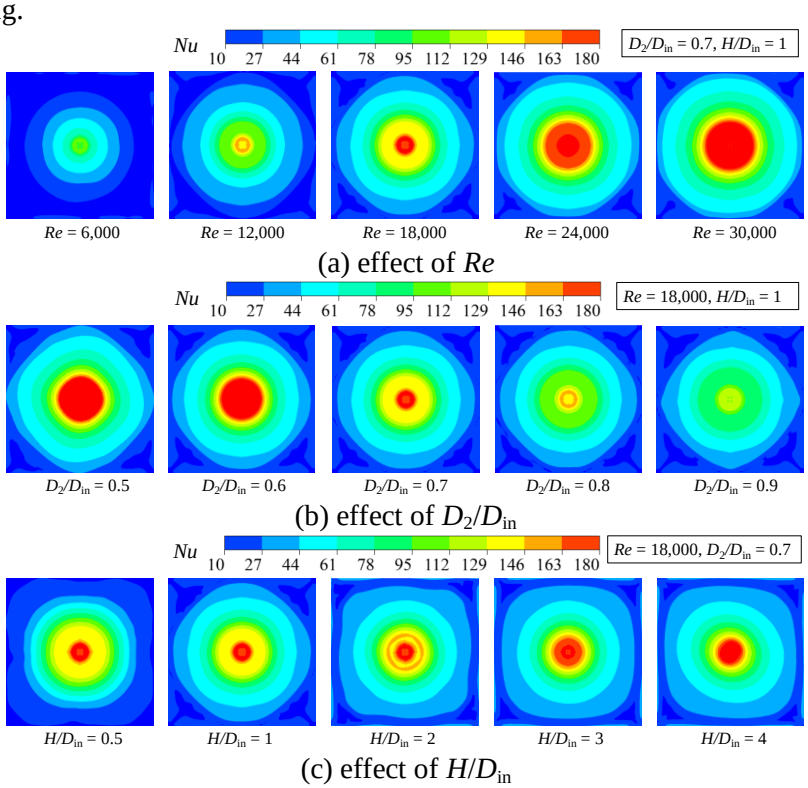

Fig. 7 Heat transfer distribution of converging-hole impinging cooling

Fig. 8 shows the change curves of *Nu* and Nu_{ave} of converging-hole impinging cooling under different parameters. It is demonstrated in Fig. 8(a) that the *Nu* distribution laws of converging-hole impinging cooling are basically the same at different *Re*. With the increment of *Re*, the *Nu* of converging-hole impinging cooling significantly increases. When the *Re* raises from 6,000 to 18,000, the increase range of *Nu* of converging-hole impinging cooling is relatively large. When the *Re* increases from 18,000 to 30,000, the increase range of *Nu* of converging-hole impinging cooling is relatively smaller. As depicted in Fig. 8(a), with the increment of *Re*, the Nu_{ave} of converging-hole impinging cooling gradually increases, and the increase rate gradually decreases. Compared with *Re* = 6,000, the Nu_{ave} of converging-hole impinging cooling at *Re* = 30,000 is increased by about 1.62 to 2.65 times under different structural parameters. As demonstrated in Fig. 8(b), the *Nu* distribution laws of converging-hole impinging cooling are similar at different D_2/D_{in}, and the main difference is that there is a significant difference in *Nu* at the high heat transfer region. Specifically, in the ranges of R/D_{in} < -2 and R/D_{in} > 2, the D_2/D_{in} inconspicuously impacts the *Nu* of converging-hole impinging cooling. However, in the range of -2 < R/D_{in} < 2, the increase of D_2/D_{in} significantly weakens the *Nu* of converging-hole impinging cooling, but the weakening extent is reduced. It can also be found in Fig. 8(b) that with the increment of D_2/D_{in}, the Nu_{ave} of converging-hole impinging cooling gradually decreases, and the decrease amplitude also gradually decreases. Compared with D_2/D_{in} = 0.5, the Nu_{ave} of converging-hole impinging cooling at D_2/D_{in} = 0.9 at different *Re* is decreased by 43.61% to 60.07%. As displayed in Fig. 8(c), the *Nu* distribution laws of converging-hole impinging cooling are not completely consistent under different H/D_{in}. When H/D_{in} is 0.5 to 3, the *Nu* distribution curves are double peak, while when H/D_{in} is 4, the *Nu* distribution curve becomes single peak. In addition, in the

ranges of -3.1 < R/D_{in} < -1.2 and 1.2 < R/D_{in} < 3.1, the *Nu* corresponding to H/D_{in} of 0.5 is higher than that corresponding to H/D_{in} of 1 to 4. In the ranges of R/D_{in} < -3.1 and R/D_{in} > 3.1, the *Nu* corresponding to H/D_{in} of 0.5 is lower than that corresponding to H/D_{in} of 1 to 4. As also displayed in Fig. 8(c), with the increase of H/D_{in}, the Nu_{ave} of converging-hole impinging cooling under different *Re* all shows slow decreasing trends. Compared with H/D_{in} of 0.5, the Nu_{ave} of converging-hole impinging cooling at H/D_{in} of 4 is reduced by about 1.06% to 6.25%, under different *Re*. Therefore, the H/D_{in} has little effect on the heat transfer capability of converging-hole impinging cooling.

4.4. Comprehensive thermal performance analysis of converging-hole impinging cooling

Fig. 9 shows the curves of *G* of converging-hole impinging cooling under different parameters. As displayed in Fig. 9(a), the *G* of converging-hole impinging cooling under different structural parameters increase with the increment of *Re*. It is because that the change rate of Nu_{ave} with respect to *Re* is greater than the change rate of C_p with respect to *Re*. Compared with *Re* = 6,000, the *G* of converging-hole impinging cooling at *Re* = 30,000 under different structural parameters is increased by about 1.58 to 2.45 times. As demonstrated in Fig. 9(b), when *Re* = 6,000 and 12,000, the *G* of converging-hole impinging cooling gradually increases with the increment of D_2/D_{in}. When *Re* = 18,000 and 24,000, the *G* of converging-hole impinging cooling slightly decreases at first and then gradually increases with the increment of D_2/D_{in}. When *Re* = 30,000, the *G* of converging-hole impinging cooling first raises and then drops with the increment of D_2/D_{in}. The reason for the inconsistency is that the change rates of Nu_{ave} and C_p are not consistent at different D_2/D_{in}. As illustrated in Fig. 9(c), the variations of the *G* of converging-hole impinging cooling with H/D_{in} are not completely consistent under different *Re*. But overall, the change curves of *G* are relatively flat, with a maximum change range of less than 4%. This shows that the impinging height ratio inconspicuously affects on the comprehensive thermal performance of converging-hole impinging cooling.

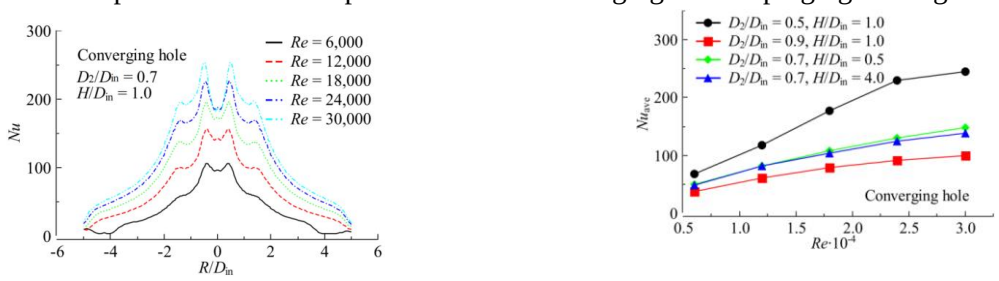

(a) effect of *Re*

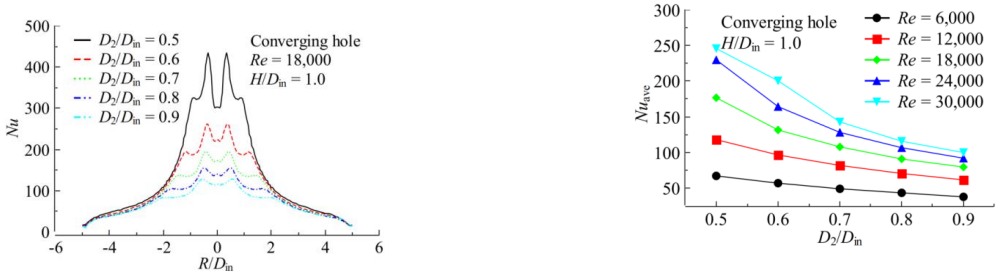

(b) effect of D_2/D_{in}

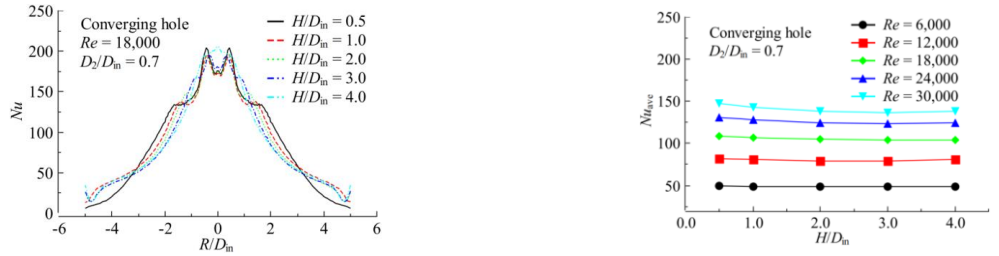

(c) effect of H/D_{in}

Fig. 8 Variation curves of *Nu* and Nu_{ave} of converging-hole impinging cooling

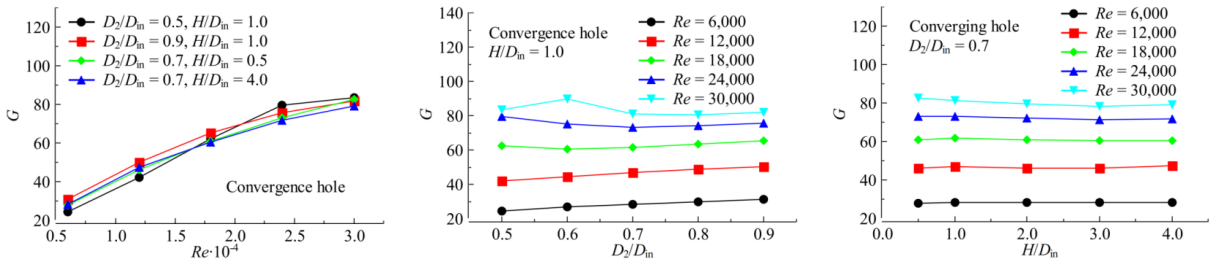

(a) effect of *Re* (b) effect of D_2/D_{in} (c) effect of H/D_{in}

Fig. 9 Variations of comprehensive thermal coefficient of converging-hole impinging cooling

4.5. Empirical correlations fitting

In order to facilitate the application of the research results of this study in the field of turbine blade cooling technology, the empirical correlations of Nu_{ave}, C_p, and G of the straight-hole and converging hole impinging cooling were fitted. Due to the poor effect of expanded hole, the empirical correlation fitting in this study was only for straight hole and converging hole, that is, the range of outlet-to-inlet diameter ratio is $0.5 \le D_2/D_{in} \le 1$. Because the variation laws of Nu_{ave}, C_p, and G of the straight-hole impinging cooling and converging hole with Reynolds number, outlet-to-inlet diameter ratio and impinging height ratio are relatively simple, the power function [3] widely utilized in literature was adopted to fit the correlations.

According to the 50 sets of calculation results of the impinging cooling using straight and converging holes in this study, empirical correlation fitting was performed using the curve_fit module in Python software. The specific fitting results are expressed as:

$$Nu_{ave} = 0.0727Re^{0.689}(D_2/D_{in})^{-1.474}(H/D_{in})^{-0.0368} \quad (6)$$

$$C_p = 0.345Re^{0.126}(D_2/D_{in})^{-4.454}(H/D_{in})^{-0.0337} \quad (7)$$

$$G = 0.119Re^{0.633}(D_2/D_{in})^{0.0667}(H/D_{in})^{-0.0232} \quad (8)$$

The application ranges of empirical correlations (6) to (8) is: $6{,}000 \le Re \le 30{,}000$, $0.5 \le D_2/D_{in} \le 1$, $0.5 \le H/D_{in} \le 4$. The maximum fitting deviations of the three empirical correlations (Nu_{ave}, C_p, and G) are 17.38%, 15.33%, and 16.17%, respectively, and the average fitting deviations are 5.73%, 8.78%, and 5.66%, respectively.

4.6. Analysis of parameter sensitivity

Sensitivity analysis is an approach that studies the extent to which changes in input variables affect output variables. Through sensitivity analysis, it can determine the importance of each input variable on the output variable, where a higher sensitivity index indicates a more important input variable. In this study, the widely applied Sobol approach on the basis of variance decomposition was adopted to execute the sensitivity analysis on the flow and heat transfer performance of the jet impinging cooling using variable-diameter holes. The Sobol approach can simultaneously compute the total sensitivity index, first order sensitivity index, and second order sensitivity index of each input variable [30].

The total variance (D) of output variable can be defined as:

$$D = \sum_i D_i + \sum_{i \ne j} D_{i,j} + \cdots + \sum_{i \ne j \ne \cdots \ne n} D_{i,j,\cdots,n} \quad (9)$$

where D_i represents the variance contribution of i-th input variable to output variable; $D_{i,j}$ represents the variance contribution of the interaction between i-th and j-th input variables to output variable; $D_{i,j,\cdots,n}$ represents the variance contribution of interactions among all input variables to output variable.

The calculation formula for first order sensitivity index S_i can be written as:

$$S_i = D_i/D \tag{10}$$

The calculation formula for second order sensitivity index $S_{i,j}$ can be written as:

$$S_{i,j} = D_{i,j}/D \tag{11}$$

Total sensitivity index S_{Ti} is the sum of the sensitivity indices of all orders, and it is given as:

$$S_{Ti} = S_i + S_{i,j} + \cdots + S_{i,j,\cdots,n} \tag{12}$$

where $S_{i,j,\cdots,n}$ represents the higher-order sensitivity indices.

Fig. 10 shows the sensitivity index distribution of performance variables (Nu_{ave}, C_p, and G) of the converging-hole impinging cooling to input variables (Re, D_2/D_{in} and H/D_{in}). Fig. 10(a) shows that for the Nu_{ave} of converging-hole impinging cooling, the first order sensitivity index of D_2/D_{in} is the highest, followed by the first order sensitivity index of Re, followed by the second order sensitivity index of the interaction between Re and D_2/D_{in}. While the sensitivity indices of other single parameters or the sensitivity indices of the interactions between other two parameters can be almost ignored. Fig. 10(b) presents that for the C_p of converging-hole impinging cooling, the first order sensitivity index of D_2/D_{in} is also the highest, while the first order and second order sensitivity indices of other terms are very low. Fig. 10(c) displays that for the G of converging-hole impinging cooling, the first order sensitivity index of Re is the highest, and the first order and second order sensitivity indices of other terms are almost negligible. Comprehensive analysis of Fig. 10(a), 10(b) and 10(c) shows that the first order sensitivity index of each performance variable to each input variable is significantly greater than the second order sensitivity index. This shows that the direct influence of the input variables on the heat transfer performance, flow performance, and comprehensive thermal performance of converging-hole impinging cooling is absolutely dominant, while the interaction of the two input variables has little influence on the heat transfer performance, flow performance, and comprehensive thermal performance of converging-hole impinging cooling. The results of Fig. 10(d) illustrates that the Nu_{ave} of converging-hole impinging cooling has the highest total sensitivity index to D_2/D_{in}, has the higher total sensitivity index to Re, and has low total sensitivity index to the H/D_{in}. This shows that the D_2/D_{in} has the greatest effect on the heat transfer performance of converging-hole impinging cooling, followed by Re, while the H/D_{in} has little effect on the heat transfer performance of converging-hole impinging cooling. The C_p of converging-hole impinging cooling is very sensitive to the change in D_2/D_{in}, and its total sensitivity index is more than 0.99. However, the C_p of converging-hole impinging cooling is not sensitive to the changes in Re and H/D_{in}. Therefore, the D_2/D_{in} has the greatest effect on the flow performance of converging-hole impinging cooling, while the Re and H/D_{in} have little influence on the flow performance of converging-hole impinging cooling. The G of converging-hole impinging cooling is very sensitive to the change in Re, and its total sensitivity index is more than 0.99, but it is not sensitive to the changes in D_2/D_{in} and H/D_{in}. This shows that Re has the greatest influence on the comprehensive thermal performance of converging-hole impinging cooling, while the D_2/D_{in} and H/D_{in} exhibit little effect on the comprehensive thermal performance of the converging-hole impinging cooling. The results of the parameter sensitivity analysis guide us in designing converging-hole impingement cooling for turbine blades, indicating that when considering exclusively on enhancing heat transfer or minimizing flow resistance, the selection of suitable hole outlet-to-inlet diameter ratio should be primarily focused. When considering both heat transfer and flow performance (i.e. comprehensive thermal performance), it is essential to focus primarily on choosing an appropriate Reynolds number.

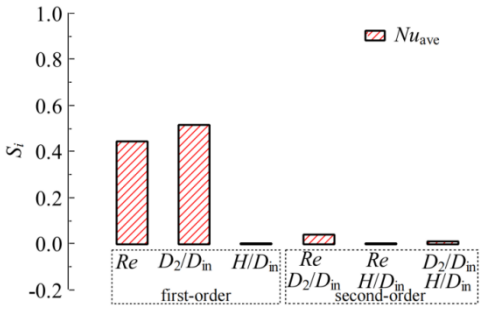

(a) local sensitivity index of Nu_{ave}

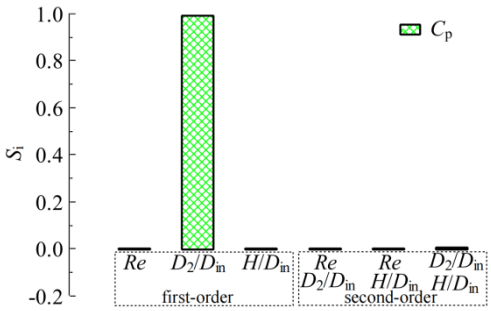

(b) local sensitivity index of f

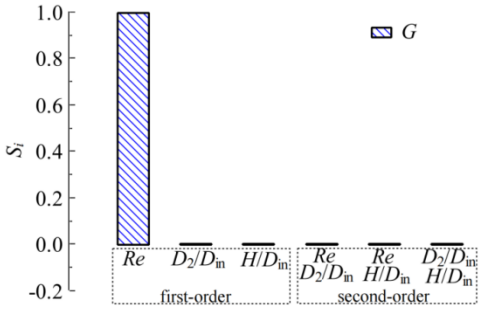

(c) local sensitivity index of G

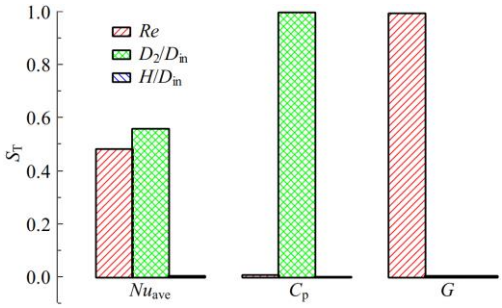

(d) total sensitivity index

Fig. 10 Distribution of parameter sensitivity indices

5. Conclusions

The heat transfer and flow performance of jet impinging cooling with three different hole configurations were studied numerically in this paper. The interesting findings have been gained:

(1) Among the jet impinging cooling of the three types of holes, the converging hole exhibits the superlative heat transfer performance but the poorest flow performance. The straight hole shows moderate levels of both heat transfer and flow performance. The expanded hole exhibits the poorest heat transfer performance but the superlative flow performance.

(2) When Re < 24,000, the expanded-hole impinging cooling shows the superlative comprehensive thermal performance, next is the straight-hole impinging cooling, and the converging-hole impinging cooling has the poorest comprehensive thermal performance. When Re > 24,000, the comprehensive thermal performance of the three types of hole configurations is similar. This may be because when Re > 24,000, the influence of Reynolds number on the comprehensive thermal performance is dominant, rather than the shape of the holes.

(3) The increase in Reynolds number has little influence on the flow performance of the converging-hole impinging cooling. Increasing hole outlet-to-inlet diameter ratio effectively improves the flow performance of the converging-hole impinging cooling. When H/D_{in} = 2.0, the converging-hole impinging cooling has better flow performance. Therefore, a lager hole outlet-to-inlet diameter ratio and H/D_{in} = 2 are suitable for situations where the mass flow rate of cold air is insufficient and flow performance needs to be improved, for the converging-hole impinging cooling.

(4) An increase in the Reynolds number effectively boosts the heat transfer performance of the converging-hole impingement cooling, whereas an increase in the hole outlet-to-inlet diameter ratio notably diminishes the heat transfer performance of the converging-hole impingement cooling. The H/D_{in} has trivial influence on the heat transfer performance of the converging-hole impinging cooling.

(5) Increasing the Reynolds number leads to a significant improvement in the comprehensive thermal performance of the converging-hole impingement cooling, whereas increasing the hole outlet-to-inlet diameter ratio and the impinging height ratio has a marginal effect on the comprehensive thermal performance of the converging-hole impingement cooling.

(6) The sensitivity analysis results indicate that when considering exclusively on enhancing heat transfer or minimizing flow resistance, the selection of suitable hole outlet-to-inlet diameter ratio

should be primarily focused. When considering both heat transfer and flow performance, it is essential to focus primarily on choosing an appropriate Reynolds number.

Acknowledgements

This research was funded by the Xi'an Jiaotong University Basic Research Business Fee Free Exploration Project (xzy012023071) and National Key Research and Development Program of China (2021YFF0602301).

References

[1] Yang, J., *et al.*, Numerical Simulations and Optimizations for Turbine-Related Configurations, *Therm. Sci.*, *24* (2020), 1, pp. 367-378

[2] Xi, L., *et al.*, Study on Flow and Heat Transfer Characteristics of Cooling Channel Filled with X-Shaped Truss Array, *Therm. Sci.*, *27* (2023), pp. 739-754.

[3] Xi, L., *et al.*, Numerical investigation and parameter sensitivity analysis on flow and heat transfer performance of jet array impingement cooling in a quasi-leading-edge channel, *Aerospace*, *9* (2022), 87.

[4] Wu, W., *et al.*, Leading edge impingement cooling analysis with separators of a real gas turbine blade, *Appl. Therm. Eng.*, *208* (2022), pp. 118275.

[5] Fan, X., *et al.*, Cooling Methods for Gas Turbine Blade Leading Edge: Comparative Study on Impingement Cooling, Vortex Cooling and Double Vortex Cooling, *Int. Commun. Heat Mass*, *100* (2019), pp. 133-145.

[6] Forster, M., *et al.*, Experimental and Numerical Investigation of Jet Impingement Cooling onto a Concave Leading Edge of a Generic Gas Turbine Blade, *Int. J. Therm. Sci.*, *164* (2021), pp. 106862.

[7] Ekkad, S.V., *et al.*, A Modern Review on Jet Impingement Heat Transfer Methods, *J. Heat Trans-T Asme*, *143* (2021), pp. 064001.

[8] Liu, K., *et al.*, A novel multi-stage impingement cooling scheme—Part ii: Design optimization, *J Turbomach*, *142* (2020), pp. 121009.

[9] Xu, L., *et al.*, Numerical simulation of swirling impinging jet issuing from a threaded hole under inclined condition, *Entropy*, *22* (2019), pp. 15.

[10] Oliveira, A.V.S., *et al.*, Experimental study of the heat transfer of single-jet impingement cooling onto a large heated plate near industrial conditions, *Int. J. Heat Mass Trans.*, *184* (2022), pp. 121998.

[11] Salem, A.R., *et al.*, Experimental and numerical study of jet impingement cooling for improved gas turbine blade internal cooling with in-line and staggered nozzle arrays, *J Energ Resour-Asme*, *143* (2021), pp. 012103.

[12] Plant, R.D., *et al.*, A Review of Jet Impingement Cooling, International Journal of Thermofluids, *17* (2023), pp. 100312.

[13] Pawar, S., *et al.*, The impingement heat transfer data of inclined jet in cooling applications: a review, *J Therm Sci*, *29* (2020), pp. 1-12.

[14] Singh, P., *et al.*, Study of flow field and heat transfer characteristics for an interacting pair of counter-rotating dual-swirling impinging flames, *Int. J. Therm. Sci.*, *144* (2019), pp. 191-211.

[15] Yang, T., *et al.*, Comparative study on flow and heat transfer characteristics of swirling impingement jet issuing from different nozzles, *Int. J. Therm. Sci.*, *184* (2023), pp. 107914.

[16] Nourin, F.N., *et al.*, Review of gas turbine internal cooling improvement technology, *J Energ Resour-Asme*, *143* (2021), pp. 080801.

[17] Tepe, A Ü., *et al.*, Experimental and numerical investigation of jet impingement cooling using extended jet holes, *Int. J. Heat Mass Trans.*, *158* (2020), pp. 119945.

[18] Zhou, J., *et al.*, Numerical investigation on flow and heat transfer characteristics of single row jet impingement cooling with varying jet diameter, *Int. J. Therm. Sci.*, *179* (2022), pp. 107710.

[19] Marzec, K., *et al.*, Heat transfer characteristic of an impingement cooling system with different nozzle geometry, *Journal of Physics: Conference Series. IOP Publishing*, *530* (2014), pp. 012038.

[20] Shuja, S.Z., *et al.*, Jet impingement onto a tapered hole: influence of jet velocity and hole wall velocities on

heat transfer and skin friction, *Int j Numer Meth Fl*, *60* (2009), pp. 972-991.
[21] Carcasci, C., *et al.*, Experimental Investigation of a Leading Edge Cooling System With Optimized Inclined Racetrack Holes, *Turbo Expo: Power for Land, Sea, and Air. American Society of Mechanical Engineers*, *45714* (2014), pp. V05AT12A034.
[22] Ram, C., *et al.*, Computational study of leading edge jet impingement cooling with a conical converging hole for blade cooling, *ARPN J. Eng. Appl. Sci*, *12* (2017), pp. 6397-6406.
[23] Sivamani, S., *et al.*, Numerical analysis of jet impingement cooling using converging conical hole for blade leading edge, *Gas Turbine India Conference. American Society of Mechanical Engineers*, *58509* (2017), pp. V001T03A009.
[24] Sathish, S., *et al.*, Influence of converging conical hole angles on jet impingement blade cooling of gas turbine blade leading edge, *AIP Conference Proceedings 6 January 2022*, *2385* (2022), pp. 120003.
[25] Zielinski, A.J., *et al.*, Impingement Cooling Using a Variable-Diameter Synthetic Jet, *17th IEEE Intersociety Conference on Thermal and Thermomechanical Phenomena in Electronic Systems (ITherm)*. IEEE, *17* (2018), pp. 429-435.
[26] Zielinski A.J., *et al.*, Flow Analysis of the Impingement of a Variable-Diameter Synthetic Jet, *J Flow Vis Image Pro*, *26* (2019), 2, pp. 127-148.
[27] Chi, Z., *et al.*, Geometrical optimization of nonuniform impingement cooling structure with variable-diameter jet holes, *Int. J. Heat Mass Trans.*, *108* (2017), pp. 549-560.
[28] Xu, L., *et al.*, Flow and heat transfer characteristics of a swirling impinging jet issuing from a threaded nozzle, *Case Stud. Therm. Eng.*, *25* (2021), pp. 100970.
[29] He, J., *et al.*, Heat transfer enhancement of impingement cooling by different crossflow diverters, *J. Heat Trans-T Asme*, *144* (2022), 4, pp. 042001.

Submitted: 09.1.2024.
Revised: 20.3.2024.
Accepted: 29.3.2024.